Geophys. J. Int. (2003) **155,** 653–668

The use of instantaneous polarization attributes for seismic signal detection and image enhancement

M. Schimmel and J. Gallart

Institute of Earth Sciences—CSIC, c/ Lluis Sole i Sabaris, s/n, 08028 *Barcelona, Spain. E-mail: schimmel@ija.csic.es*

Accepted 2003 July 4. Received 2003 July 4; in original form 2002 May 23

SUMMARY

This paper introduces and discusses a new polarization filter which can aid interpretation of single or multichannel multicomponent seismograms. We define a measure of degree of polarization based on instantaneous polarization attributes of analytic traces. Computation of the data eigenstructure is not required and the measure can be used in combination with its spatial coherence to enhance polarized signals on seismic record sections. Our approach avoids suppressing signals with spatially changing characteristics such as happens in the transition to post-critical reflections or for reflections from laterally varying interfaces. The simplicity of the method permits the filter to be tailored to various data characteristics and the concept can be applied to cross-energy methods. We also show that non-linear amplification of rectilinearity and planarity weight functions in time-domain principal-component filters permits the size of data windows to be decreased, improving resolution and suppressing noise.

Key words: polarization, seismic noise, seismic-phase identification, seismograms.

1 INTRODUCTION

The study of signal detection and enhancement is motivated by the goal of extracting more information from small energy signals to constrain the fine structure of the Earth. However, signal and noise often share similar amplitudes, frequencies, waveforms and/or other characteristics. When there is no clear separation between signals and noise, it is difficult to establish objective criteria for how best to enhance the signals.

This paper deals with signal enhancement using triaxial data systems through a time-domain degree of polarization filter. Where densely spaced data are available, the filter can incorporate the spatial coherence of the degree of polarization for further noise suppression. To aid seismic interpretation, interfering signals such as multiple reverberations or reflections from subsurface scatterers are often classified as signal-generated noise and ideally should be suppressed just like other noise during data processing. Signal-correlated noise can exhibit partial spatial coherence and resembles the signals in most characteristics. It is therefore often the most difficult noise to eliminate. Directional coherence measurements (for example, Stoffa *et al.* 1981; Kong *et al.* 1985; Duncan & Beresford 1994; Schimmel & Paulssen 1997; Kennett 2000) and/or polarization analyses (for example, Montalbetti & Kanasewich 1970; Samson 1983; Christoffersson *et al.* 1988; Perelberg & Hornbostel 1994; Du *et al.* 2000; Reading *et al.* 2001) are helpful tools for attenuating noise, including signal-generated noise.

Directional coherence measurements exploit the spatial coherence and enhance the signal wavefield by suppressing incoherent signals and coherent signals with energy outside specified apparent velocity (equivalently, slowness or wavenumber) ranges. There are various approaches that operate in the time–distance, frequency–wavenumber or intercept–slowness domains. The domain that best separates the signal from the noise should be preferred in the data processing.

Polarization analysis makes full use of the three-component vector field to characterize the particle motion. Polarization attributes are usually derived in the frequency domain (for example, Samson 1983; Park *et al.* 1987) or in the time domain (for example, Kanasewich 1981; Bataille & Chiu 1991). The frequency domain approaches are most efficient for dispersed or superimposed waves of distinct frequency content. If, however, the signals are separated in time and exhibit similar spectral characteristics then time-domain approaches are recommended. Some approaches are time–frequency domain hybrids (Jurkevics 1988); others employ analytic signals (Taner *et al.* 1979) rather than real time-series to obtain instantaneous polarization attributes (Vidale 1986; Bataille & Chiu 1991; Morozov & Smithson 1996, among others).

Independently of their domain, most algorithms rely on the eigenanalysis of the data covariance matrix (in the frequency domain also called the spectral density matrix). The covariance matrices are determined for sliding time windows, which should be long enough to permit noise attenuation but which should not include multiple signals. Multitaper algorithms can be employed to diminish spectral leakage if required (Park *et al.* 1987). The eigenanalysis provides a decomposition of the windowed data into their principal energy components (Samson 1983; Jackson *et al.* 1991) given by eigenvalue–eigenvector pairs. The eigenvalues are the energy components and the eigenvectors are the corresponding principal directions. Linear or elliptical motions are projected on to one or two principal directions, respectively. Rotation of the triaxial data into the eigenvector

frame is called principal-component transformation and can be obtained directly by singular-value decomposition (SVD) of the data matrix (Jackson *et al.* 1991). This rotation is the basis for many polarization filters.

The directional coherence measure and principal-component analysis can be combined when using densely spaced data (Samson & Olson 1981; Jurkevics 1988; Bataille & Chiu 1991). To take advantage of spatial signal coherence, following time alignment either the triaxial recordings or the covariance matrices are averaged. Depending on the window size, averaging covariance matrices requires less accuracy in the time alignment than first stacking the data. Both methods improve the resolution of the polarization attributes, but attenuate polarized signals with spatially changing characteristics.

In the following we present and discuss a new method to enhance signals by noise attenuation using instantaneous polarization attributes. The data windows used in our approach can be very small so they enable good signal resolution. Furthermore, dealing with multichannel data, we obtain in combination with a directional coherence measure a 2-D filter that can enhance the polarized signals and which is invariant to phase or polarization changes at various offsets. Signal-generated noise with a low degree of polarization and/or unexpected apparent velocities is suppressed by the filter. The method is quite simple so permits several extensions to aid seismogram interpretation. We test the approach with synthetic data and compare it with a powerful eigenapproach that uses a weighted eigenimage composition of the three-component seismograms (De Franco & Musacchio 2001). We slightly extend their approach to enable the use of shorter data windows and to facilitate comparison with our method. Finally, we apply the filter to a record section of the Ligurian Sardinian (LISA) wide-angle seismic profile, which was used by Gallart *et al.* (2001) to study the onshore–offshore crustal transect in the eastern Pyrenees.

2 METHODOLOGY

First, we briefly review the analytic signal and its use for determining instantaneous polarization vectors for three-component seismic records. The polarization vectors describe the instantaneous orientation of the semi-major and semi-minor axes of an ellipse that represents the signal motion in 3-D space. We will use a new approach and explain how these axes can be employed to define the degree of polarization and to suppress signals that are less polarized. The method is an alternative to principal-component analysis and can enhance signals of elliptical and linear motion without assuming any predefined polarization or direction. It is straightforward and easily comprehensible, permitting various extensions such as directional filtering.

2.1 Analytic signal and instantaneous signal polarization

The complex signal or trace $u^c(t)$

$$u^c(t) = u(t) + i\,H[u(t)] = A(t)\exp\left[i\,\Phi(t)\right] \tag{1}$$

is uniquely defined by the real time-series $u(t)$ and its Hilbert transform $H[u(t)]$ and can be expressed as a real-valued amplitude vector $A(t)$ and a real phase function $\Phi(t)$. These last two functions are called the envelope and instantaneous phase (Taner *et al.* 1979). The analytic signal is advantageous since it factorizes the signal as a function of time into a low-frequency envelope function and a high-frequency phase function. This is obtained without explicitly performing a moving window analysis as required by time–frequency analyses. Indeed, a moving window is implicitly included through the Hilbert transform which locally weights the time-series. The transform applies a phase shift of $\pi/2$ to obtain the orthogonal complex part of the analytic signal. The analytic trace enables the direct determination of trace attributes on a sample by sample basis and hence can be exploited to obtain the instantaneous polarization of three-component (or general multicomponent) signals.

To compute the instantaneous polarization one needs to build an analytic signal vector

$$\mathbf{B}(t) = \left[u_1^c(t), u_2^c(t), u_3^c(t)\right] \tag{2}$$

from the three-component seismic record, where $u_i^c(t)$ denotes the analytic signal of the ith component seismogram. Following Vidale (1986), $\mathbf{B}(t)$ can be used to compute the instantaneous covariance matrix and its eigenstructure. Bataille & Chiu (1991) have shown that it is sufficient to use the real part of the instantaneous covariance matrix since the principal directions can be considered to be real. They further stress that instantaneous covariance matrices provide eigenvalues that are invariant to constant signal phase shifts.

Instantaneous polarization attributes can also be determined directly as shown by Morozov & Smithson (1996). Their approach is based on the factorization of the analytic vector $\mathbf{B}(t)$

$$\mathbf{B}(t) = \mathbf{C}(t)\exp[i\,\Psi(t)] \tag{3}$$

into one single real-valued phase $\Psi(t)$ and a complex-valued vector function $\mathbf{C}(t)$ with amplitude, polarization and phase-shift information. The phase function is obtained directly through a variational approach that maximizes the form $\sum_k \{\mathrm{Re}[\exp(-i\,\psi)u_k^c(t)]\}^2$ together with a small regularization term which stabilizes the calculation when the first term becomes constant. Semi-major $\mathbf{a}(t)$ and semi-minor $\mathbf{b}(t)$ axes are easily extracted from the complex vector $\mathbf{C}(t)$. Since $\Psi(t)$ is determined with a phase uncertainty of π the sign of the axes is unknown. Besides the phase uncertainty the vectors $\mathbf{a}(t)$ and $\mathbf{b}(t)$ describe the ground motion, which is always represented by an ellipse lying in a plane in the 3-D space (Morozov & Smithson 1996).

2.2 Degree of polarization measure

We now define polarized signals as features that do not change their polarization during the duration of the signal. Constraining the definition to a particular type of polarization would lead to a directional polarization filter but that is not the aim here. A rotationally invariant measure for the degree of polarization may be constructed as

$$c(t) = \left[\frac{1}{T+1}\sum_{\tau=t-T/2}^{t+T/2}\left|\frac{\mathbf{m}(t)}{|\mathbf{m}(t)|}\cdot\frac{\mathbf{a}(\tau)}{|\mathbf{a}(\tau)|}\right|^{\nu_1}\right]^{\nu_2}. \tag{4}$$

T denotes a short data window of $T+1$ samples and $\mathbf{m}(t)$ is the mean polarization vector of the data window. The $T+1$ projections of the instantaneous unit polarization vectors are summed on to their unit mean vectors. Owing to the phase uncertainty of π, absolute values are used to avoid destructive addition through phase changes. The transition between low and high degrees of polarization is controlled by the exponents ν_1 and ν_2. This helps to increase noise attenuation when the differences between more polarized and less polarized signals are small. ν_1 and ν_2 act on the individual vector projections and their sum, respectively. It is not very important how these differences are increased and we routinely use $\nu_1 = \nu_2 = \nu$ to decrease the number of parameters. Thus, $c(t)$ is a functional that ranges between 0 and 1 with 1 indicating a homogeneously polarized signal throughout the time window T. If the semi-major axis

direction is strongly varying then the projections on to the mean vector $\mathbf{m}(t)$ become smaller and lead to a small value for $c(t)$.

Vector $\mathbf{m}(t)$ is a mean (or median) vector that characterizes the polarization in the data window. It can be tailored for different applications and statistics. For instance,

$$\mathbf{m}(t) = \frac{1}{T+1}\sum_{\tau=t-T/2}^{t+T/2}\mathbf{a}(\tau) \quad \text{or} \quad \mathbf{m}(t) = \frac{1}{T+1}\sum_{\tau=t-T/2}^{t+T/2}\frac{\mathbf{a}(\tau)}{|\mathbf{a}(\tau)|} \tag{5}$$

provide two different mean directions of the semi-major axis. The first direction is weighted by the signal amplitudes. This definition is useful for better determination of polarization attributes of large-amplitude signals. Conversely, the second mean is independent of signal amplitudes and can therefore be used to attenuate strong bias caused by large-amplitude noise. We use the second approach since we are interested in discriminating signals from their signal-generated noise independently of their amplitudes. Note that other, more specialized, low-pass filters can also be used to produce vectors $\mathbf{m}(t)$ from $\mathbf{a}(t)$ vectors normalized in other ways.

The functional $c(t)$ is defined purely as a function of the instantaneous semi-major axis. This axis is generally well defined with the exception of circular or almost circular motion. As a result of the presence of noise the possibility cannot be excluded that the instantaneous semi-minor axes of a noise-free signal are exchanged with the semi-major axes because of noise contamination. Consequently, for almost circular polarized ground motion these directions might not be stable during the signal duration. We tackle this problem by defining a planarity vector

$$\mathbf{p}(t) = \mathbf{a}(t) \times \mathbf{b}(t) \tag{6}$$

for circular or elliptical motion. $\mathbf{p}(t)$ is perpendicular to the elliptical plane of motion and should not vary if the motion stays in the same plane. This is what we expect during the course of an elliptically polarized signal and hence can be used for signal discrimination. The degree of polarization is constructed by replacing attribute $\mathbf{a}(t)$ in eqs (4) and (5) by the planarity vector $\mathbf{p}(t)$ whenever the mean of the ratio of the semi-minor to the semi-major axis becomes larger than some defined limit. We will use $c(\mathbf{a}(t), \mathbf{p}(t))$ to indicate that the degree of polarization depends on the semi-major and planarity vector. The filtered traces $f_i(u_i) = u_i(t) \cdot c(\mathbf{a}(t), \mathbf{p}(t))$ are obtained by multiplying the time-series by the instantaneous attribute. Note that the degree of polarization function is the same for all components. The amplitude ratios across the three components are therefore preserved. Moreover, the concept of 'degree of polarization', as defined here, can also be used in principal-component analysis with respect to the corresponding eigenvectors.

2.3 Examples with synthetic data

In what follows, we apply the method to synthetic data to demonstrate its ability to suppress relatively unpolarized signals. The test records in Figs 1(a) and (b) mimic broad-band (*bb*) and narrow-band (*nb*) three-component single-station data. The time-series are displayed with their sample index rather than their time values to simplify comparison with the window sizes of only a few samples. Four signals are present in each data set. Signals 1–4 have elliptical, linear, circular and elliptical polarization, respectively. The time-series have been contaminated with small- and large-amplitude noise. The noise is built in the frequency domain by ascribing a random phase spectrum to the scaled signal amplitude spectrum and is added to the data after the application of an inverse Fourier transform. The polarization filtered traces are shown in Figs 1(c) and (d). Some of the instantaneous polarization attributes are shown in Figs 1(e) and (f): from top to bottom these are the rectilinearity, the semi-major $|\mathbf{a}(t)|$, the semi-minor $|\mathbf{b}(t)|$, attributes $c(\mathbf{a}(t))$, $c(\mathbf{p}(t))$ and $c(\mathbf{a}(t), \mathbf{p}(t))$ using five (*bb* and *nb* data), seven (*bb* data) or 11 (*nb* data) sample windows. The power ν is 6 and 12 for the *bb* (Figs 1c and e) and *nb* data (Figs 1d and f), respectively. The lowermost trace is the degree of polarization employed to filter the data from Figs 1(a) and (b).

It can be seen from Figs 1(a)–(d) that the filter removed both the large and small energy noise. This is to be expected since the attribute $c(\mathbf{a}(t), \mathbf{p}(t))$ is explicitly amplitude unbiased. Figs 1(e) and (f) further show that the linearly polarized signal 2 is better detected by $c(\mathbf{a}(t))$ than by $c(\mathbf{p}(t))$. $c(\mathbf{a}(t))$ does not detect the circular motion of signal 3 due to the ambiguity already discussed of the semi-major axis associated with $\mathbf{a}(t)$. The figure shows that the circular and elliptical signals 1, 3 and 4 are best detected with $c(\mathbf{p}(t))$. Altogether, the combination of both measures into $c(\mathbf{a}(t), \mathbf{p}(t))$ enables the simultaneous detection of all signals.

From Figs 1(e) and (f), it appears that a longer data window (T in eq. 4) improves the noise attenuation. This is not generally expected to be the case, since the summation (eq. 4) in data windows that include the stretched signal, the surrounding noise and other signals may not be as effective as for windows that include only the signal or portions of it. This is partly because no negative values are permitted in the addition of the vector projections in eq. (4). Nevertheless, the window needs to be long enough to discriminate between signal and noise. In our example, with the *nb* data (Figs 1b, d and f), the five-sample window yields little suppression of the noise. The noise and the signal differ only slightly in the triaxial data system over five samples.

The dependence on window length and power in our test data is illustrated in Fig. 2. We define the signal-to-noise (S/N) energy ratio as $\mathrm{S/N} = (S_0 + S_\mathrm{f})/(N_0 + N_\mathrm{f}) \cdot n_\mathrm{f}/n_s$, where S_0, N_0 and S_f, N_f are the signal and the noise energy before and after the filter on the vertical component records and n_f and n_s are the total number of noise and signal samples, respectively. The signals are defined by their grey background in Figs 1(a) and (b). S_0 and N_0 stabilize the S/N ratio in the cases where N_f or N_f and S_f become very small. The values plotted in Figs 2(a), (c) and (d) are the mean ratios obtained for 40 different random noise realizations. The different noise realizations were obtained by ascribing random phase spectra to the scaled signal amplitude spectrum. First, we consider only the linearly polarized signal 2 and substitute small-amplitude noise for signals 1, 3, 4 (Figs 1a and b).

Fig. 2(a) shows the energy ratios of the unnormalized (*bb* and *nb*) and normalized (*bb_n* and *nb_n*) vertical component records. In Fig. 2(b) we show the vertical component filter output for different window lengths and power values.

The monotonic decrease of the *bb* and *nb* energy ratios (Fig. 2a) at the long windows beyond the maximum ratios reflects the overall decrease of the weighting attribute $c(\mathbf{a}(t), \mathbf{p}(t))$ due to the inclusion of additional noise in the analysis window. That is, S_f and N_f decrease so much that the ratio almost reaches its limit of $S_0/N_0 \cdot n_\mathrm{f}/n_s$. This may give the incorrect impression that signals cannot be detected with long windows. In fact, noise is generally more attenuated than the signals which may still permit signal detection. Therefore, the energy ratio is also shown for the amplitude normalized traces. The larger *bb_n* and *nb_n* energy ratios indicate that the signals (and noise) are not entirely suppressed by the filter. This is illustrated by the first and third trace in Fig. 2(b). These traces were obtained using seven and 49 sample windows. Their *bb* energy ratios (Fig. 2a) are

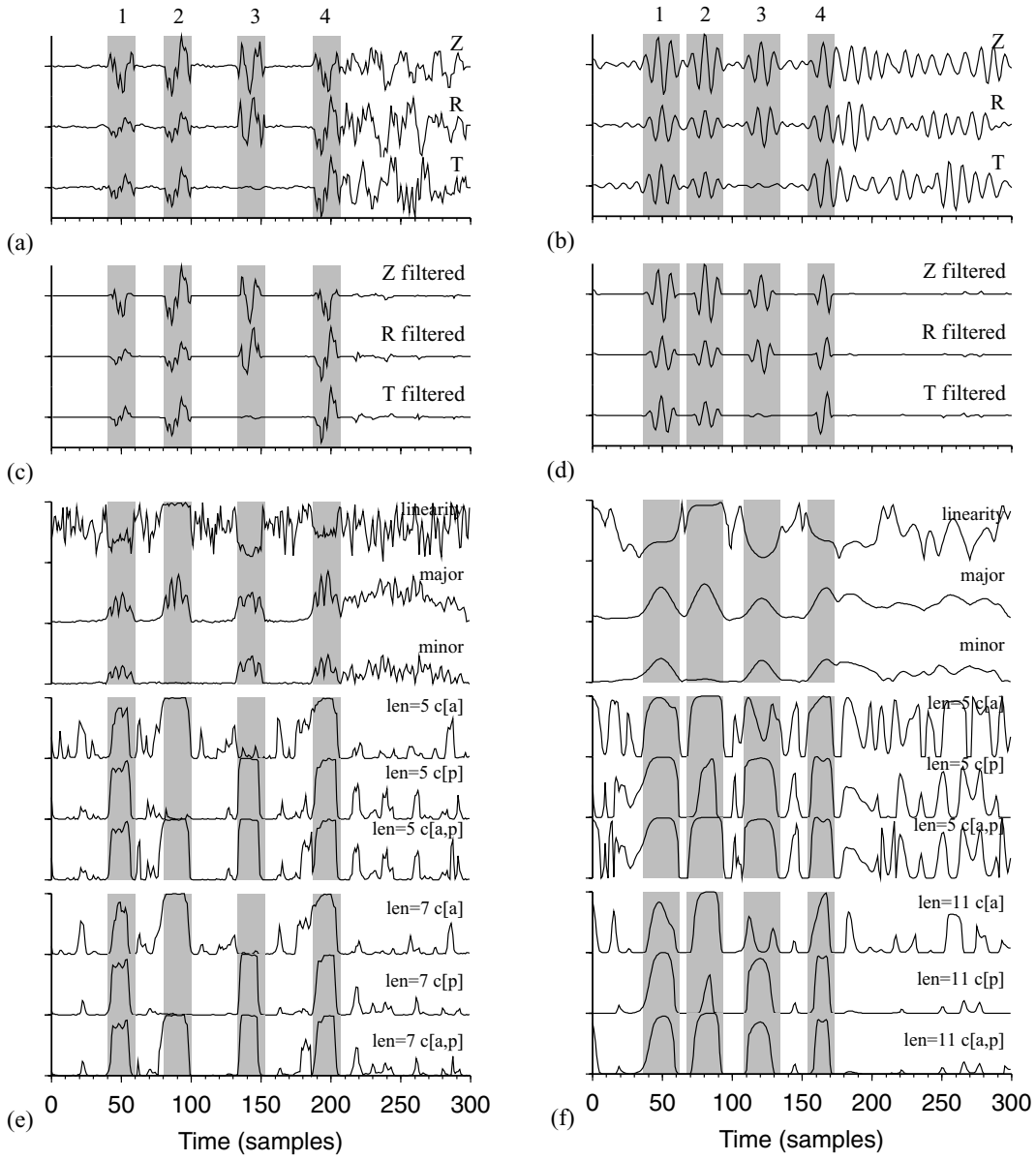

Figure 1. The three-component test data in (a) and (b) were generated with a broad (a) and narrow (b) frequency band. Numbers and the grey background mark the signals. The traces are contaminated with random noise, which is built from the signal amplitude spectrum. Parts (c) and (d) show the filtered data and (e) and (f) contain the distinct corresponding polarization attributes. The lowermost trace in (e) and (f) are the attributes used to obtain the data from (c) and (d), respectively.

quite different, but the curve *bb_n* for the normalized traces shows a similar ratio, which is consistent with their waveform semblance.

The two lowermost seismograms (Fig. 2b) are the filter outputs that correspond approximately to the maxima of the *nb* curves (Fig. 2a). The larger power value seems to increase the differences between signal and noise and thus permits use of shorter windows to obtain similar results. The fourth trace in Fig. 2(b) shows that one does not need to stick to the maximum values in order to obtain signal-enhanced seismograms.

Figs 2(c) and (d) illustrate the influence of the window length and power value on the *bb* and *nb* test data using all four signals from Fig. 1. The energy ratios have a similar trend to the curves in Fig. 2(a). We see that the window size can be quite small and that the optimum filter performance is controlled by the window length to power trade-off. The signals and noise are often difficult to separate with short windows. In these cases, larger power values can raise the differences to permit a stronger attenuation of the less polarized signals. Larger power values can therefore enable noise suppression with shorter data windows.

In Figs 3(a) and (b) we show the vertical component filter output for the test data from Figs 1(a) and (b). Various filter settings are used to demonstrate the different waveform responses. It is obvious from this figure that intermediate windows can suppress signals beginning at their start and end time. This is due to the other signal and noise components which start to affect $c(\mathbf{a}(t), \mathbf{p}(t))$ when the data window is centred at the signal beginning or end. It can make a difference whether random noise or a second distinct polarized signal enters the data window. This explains, for instance, the survival of signals 1 and 2 in Fig. 3(b) for a 49-sample window. Fig. 3 shows that the filter can be most effective at the shorter data windows. The short

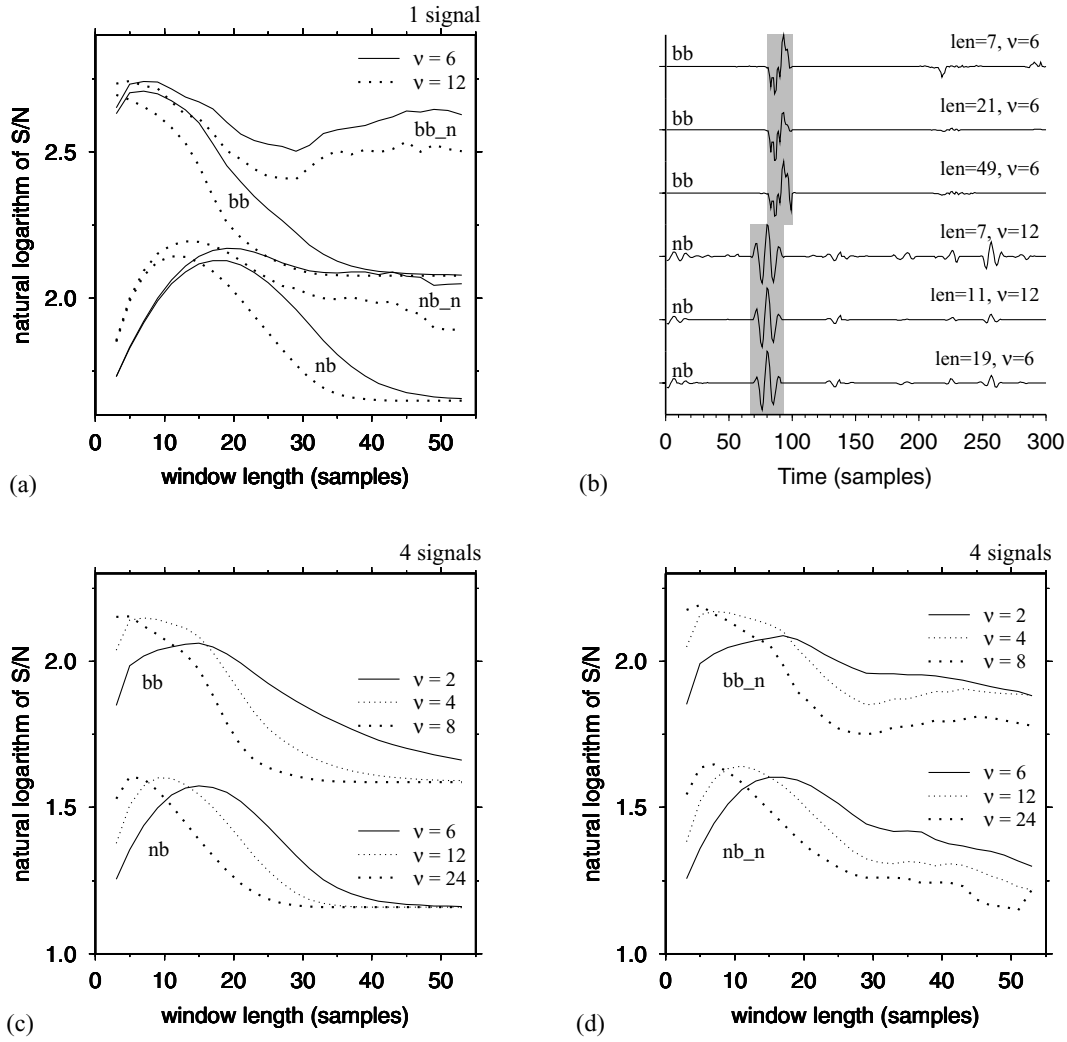

Figure 2. Dependence of window length and power using the three-component broad-band (*bb*) and narrow-band (*nb*) signals from Fig. 1 with 40 different random noise realizations. For (a) and (b) we use signal 2 and for (c) and (d) all signals. Parts (a), (c) and (d) show the mean signal-to-noise energy ratios for the filtered–unfiltered vertical component records. *bb_n* and *nb_n* indicate that the traces were normalized with respect to the trace maximum after the filter operation. The traces in (b) are filtered vertical components from the data used in (a). The filter efficiency increases at shorter windows for increasing power within a limited range of values.

windows and higher power values permit isolation of signals in the vicinity of higher-amplitude noise. This can be seen for signal 4 from the top four traces in Fig. 3(b).

2.4 Minimum signal duration and waveform preservation

To enable further signal enhancement we can discriminate signals from noise by defining the minimum duration of a polarized state. That is, we assume that the signal has a minimum duration with degree of polarization $c(\mathbf{a}(t), \mathbf{p}(t))$ larger than a defined reference value. We raise the attribute $c(\mathbf{a}(t), \mathbf{p}(t))$ to 1 whenever the corresponding sample belongs to a signal that satisfies the minimum duration condition and square the value of the attribute everywhere else. Fig. 4 shows the data from Figs 1(a) and (b) after application of the minimum signal duration algorithm. We use an analysis window of five samples and a minimum signal duration of 10 samples at a reference amplitude of 0.9^{v} to obtain the filter output in Fig. 4. For complete clean-up of short-duration signals the squared values should be replaced by zeros. Raising the selected $c(\mathbf{a}(t), \mathbf{p}(t))$ values to 1 or any other constant value ensures that the signals are not distorted. Any feature that has a degree of polarization larger than the reference value and which satisfies the minimum duration condition will not be suppressed at all. Thus some noise might not be suppressed and it can be difficult to establish good values for noisy data when one does not have *a priori* information concerning the expected signals.

This algorithm has been applied to the test data from Figs 1(a) and (b) with 40 random noise realizations with amplitude spectra matching that of the signal. The S/N energy ratio is depicted in Fig. 5(a). In comparison with Figs 2(a) and (b), it can be seen that the algorithm did not much change the course of the ratio with, however, slightly increased amplitude range. Fig. 5(b) shows that the shape of the curves does not vary greatly when increasing the noise amplitudes by a factor of 2, 3 or 4. The overall amplitudes are certainly decreased since the signal waveforms are more contaminated by noise and the signals are therefore less polarized. Consequently, polarization and signal detection generally become more ambiguous.

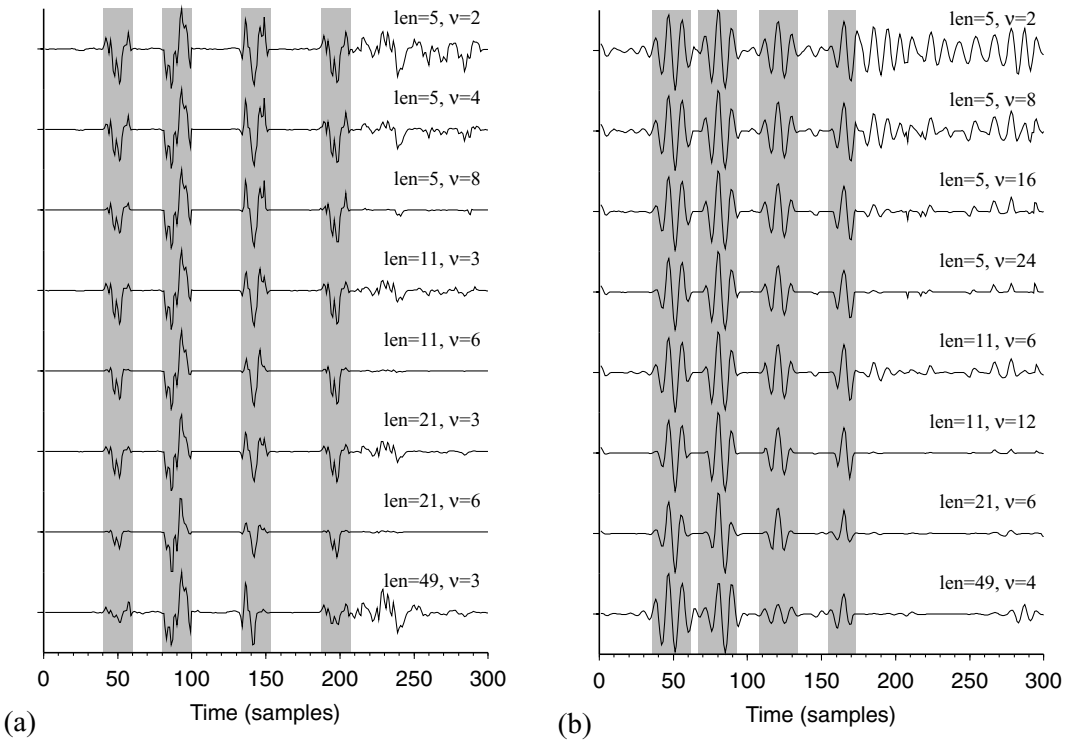

Figure 3. The three-component data from Figs 1(a) and (b) have been filtered with the distinct filter length and power (ν) values. The vertical components for the *bb* (a) and *nb* (b) data are shown.

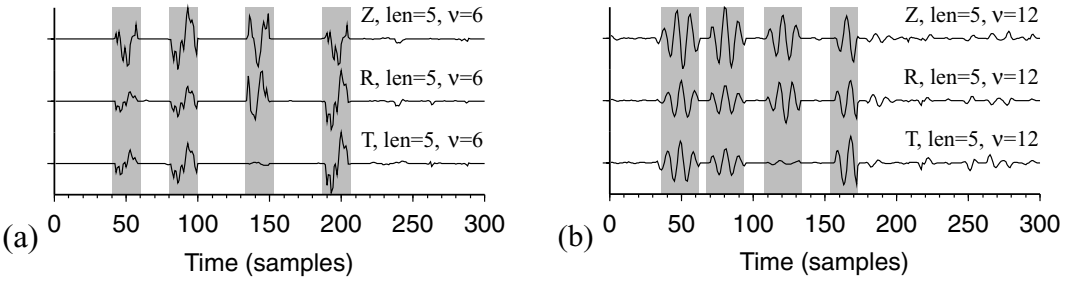

Figure 4. The three-component data of Figs 1(a) and (b) are filtered using an analysis window of five samples. The attributes are flattened using a minimum duration algorithm to avoid signal distortion and to suppress short-duration signals.

2.5 Spatial averaging of the degree of polarization

With densely spaced data the filter can be adapted to include the directivity of the wavefields, thereby increasing the filter efficiency. This is recommended in any noisy polarization analysis since the signal polarization is vulnerable to noise. For linear arrays, such as shown below, we apply the local slant stack (for example, Milkereit 1987; Duncan & Beresford 1994) to the instantaneous degree of polarization rather than to the individual seismic records themselves. This is a simple way to incorporate full triaxial data information to favour the polarized signals measured with the array. The stacks or averages of the attributes become waveform independent and punish signals with a low degree of polarization and/or without spatial attribute coherence. Since the degree of polarization method does not depend on the type of polarization the polarization of signals can change without being attenuated. This permits the detection of polarized signals with spatially changing characteristics, such as obtained in the transition to post-critical reflections or with laterally varying reflector properties. Averaging of the polarization attribute enables removal of spatially coherent signals (noise) that are less polarized, such as signal codas generated by the superposition of multiple reverberations.

The diagrams in Figs 6(a) and (b) illustrate the procedure. A sliding time–distance window (box in Fig. 6a) across the instantaneous degree of polarization section specifies the subsidiary data for the local stack. The averages (e.g. mean or median) are determined along straight lines defined by a range of slowness values. The maximum average value is assigned to the centre sample of the 2-D window, which is then moved to an adjacent sample location and the entire procedure is repeated.

To avoid the need for signals to be exactly aligned along straight-line segments and to enable some control of the minimum signal duration, a time window ΔT centred at the straight lines is used. Concerning the average, we suggest use of the median, but mean and other averages are also possible. The median is more robust than the mean to noise bursts or outliers; the mean is more affected by outliers and this blurs sharp detail. In Figs 6(c)–(e) we illustrate the differences between median and mean averaging in our algorithm.

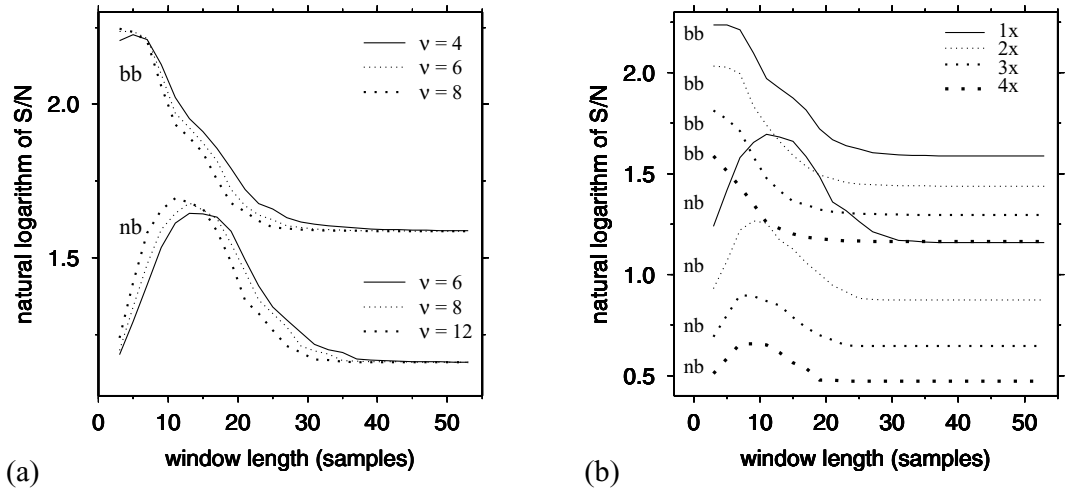

Figure 5. (a) The mean S/N energy ratio is shown for the vertical traces from Figs 1(a) and (b), but 40 different random noise realizations derived from the signal amplitude spectrum. The filter employs the minimum duration algorithm. (b) Same as (a) but the noise has been multiplied by 2, 3 and 4. The power ν is 6 (*bb*) and 12 (*nb*), respectively.

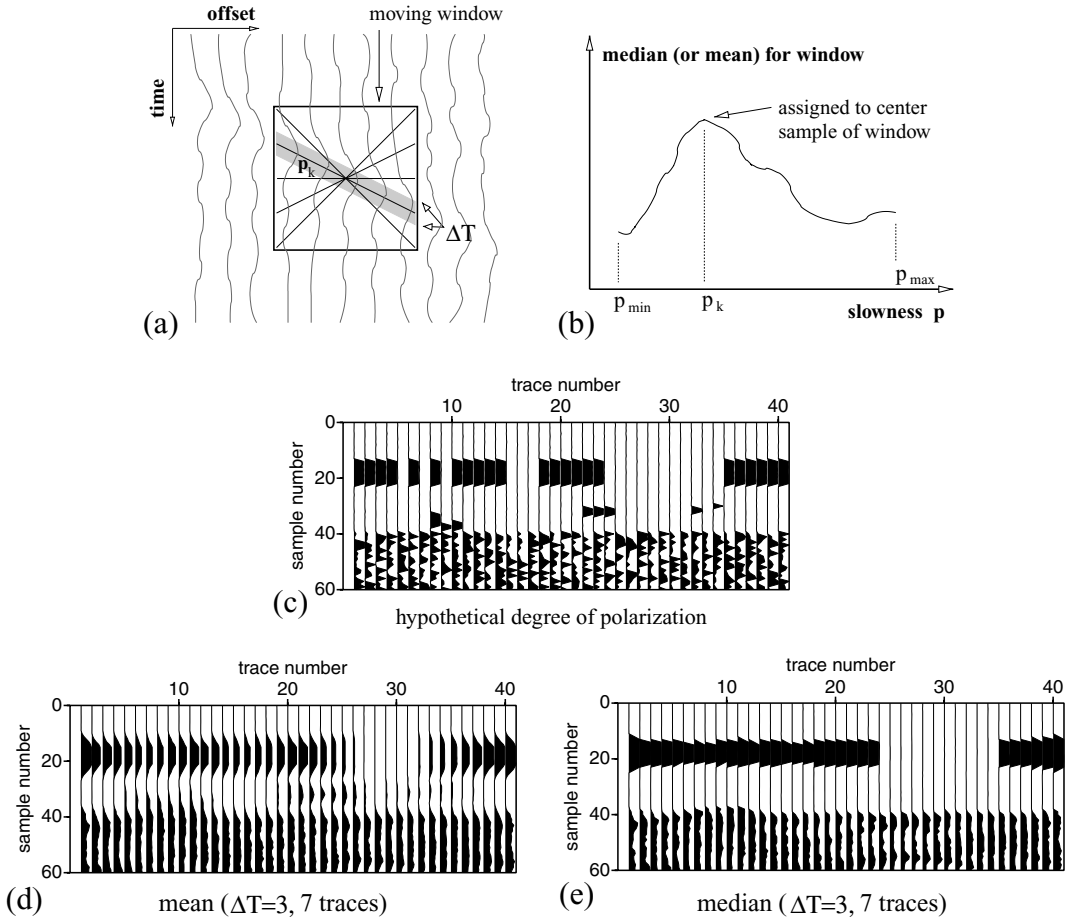

Figure 6. Illustration of local averaging of filter attributes. (a) The degree of polarization as a function of time and trace offset is locally smoothed within a moving data window. The mean or median are determined along straight trajectories with width ΔT and the different slowness values p. (b) The maximum value is assigned to the centre sample of the 2-D data window before it is moved to the next position. (c) Test attribute section and its mean (d) and median (e) filtered result. ΔT is set to three samples and the data window is seven traces wide. The isolated features at samples 30–40 (c) and the smaller gaps at sample 20 (c) may be caused by isolated polarized noise and unpolarized signals due to noise corruption, respectively. The median filter (e) preserves the edges and removes the outliers while the mean (d) blurs these features.

A hypothetical degree of polarization section is shown in Fig. 6(c). A coherent event with gaps of different sizes is located at sample 20. The smaller gaps could have been caused by unpolarized signals owing to interference from other events. Random noise is inserted at samples larger than 40. The remaining isolated signals are outliers such as might be caused by polarized noise.

The mean and median averages are shown in Figs 6(d) and (e), respectively. ΔT equals three samples and the data window is seven traces wide. It can be seen from these figures that the median better preserves the sharp edges than the mean filter. The median also removed the outliers. Whether the gaps in the signal at sample 20 are preserved or not depends on the width of the sliding 2-D data window.

The effects of applying the filter to signals with spatially changing characteristics, signal interference and random but spatially coherent noise are illustrated in the examples of Fig. 7. We use synthetic *nb* data comprised of four polarized signals with no energy in the transverse components. The vertical and radial component record sections are depicted in Figs 7(a) and (b). The transverse components contain random noise and are not shown. The first arrival at about sample 40 has elliptical polarization, which changes its phase by 3° per trace. The second signal has positive slowness, is linearly polarized and interferes with a third circular polarized signal that arrives at about sample 100. The circularly polarized signals contain two discontinuous arrival time changes. The fourth signal is located at samples 160–170. It has elliptical polarization and its amplitude on the vertical component is modulated by the absolute values of a cosine function. The signals after sample 179 are amplified random noise, but spatially coherent. The signal waveforms change laterally where the signals interfere, where the arrival time changes discontinuously, and where the polarization varies as a function of offset. The entire data have been contaminated by random noise derived from the signal amplitude spectrum.

Fig. 7(c) shows the vertical component filter output determined with local averages over 15 traces. The window length, the power ν and ΔT are set to 9, 10 and 3. The corresponding averaged degree of polarization is illustrated in Fig. 7(d). Comparison of Figs 7(a) and (c) shows that the signals with abrupt or smooth changes are not more attenuated than the other signals. It demonstrates that the averages do not punish polarized signals with laterally changing properties. Interfering signals are generally not much attenuated for two reasons: the interference of polarized signals can yield newly polarized signals and less polarized signals sandwiched between polarized signals may not be suppressed owing to the averaging.

The spatially coherent noise has almost been removed. It is not entirely removed since part of the noise is slightly polarized. If polarized noise is also coherent then it cannot be separated from a polarized signal without other *a priori* information.

Figs 7(e) and (f) show the data from Figs 7(a) and (b) with stronger noise contamination. A frequency bandpass filter cannot remove the noise since it is derived from the signal amplitude spectrum. The vertical component filter output and the averaged degree of polarization are displayed in Figs 7(g) and (h). The filter settings are the same as those of Figs 7(c) and (d). The signal degree of polarization has been decreased due to the overall unpolarization through the increased noise interference. Nevertheless, the signals are enhanced since less polarized noise has been attenuated. Further noise increases in the data would increasingly corrupt the signal polarization and deteriorate the filter output. As long as the differences in the degree of polarization values between unpolarized signals and noise are large enough there will be a stronger attenuation of the noise. If the noise becomes too large then one needs either *a priori* knowledge/estimates of the noise or to work in another domain where the signal and the noise can be separated.

3 DEGREE OF POLARIZATION FILTER COMPARED WITH AN EIGENAPPROACH

Most polarization filters are based on the eigenstructure of the data covariance matrix and are used with some design of weighting function for seismic wave-type selection (for example, Perelberg & Hornbostel 1994). A filter based on the eigenapproach to enhance both elliptical and linear motion has recently been published by De Franco & Musacchio (2001). It is an interesting method which we will employ and compare with our filter. It is not our purpose to determine a best method. In general, data properties and the application at hand are the key elements for deciding which method(s) should be used to process the data from amongst those available.

The method of De Franco & Musacchio (2001) uses the principal-component transform through a SVD to rotate the data matrix directly into the eigenvector frame. The transform is also known as the Karhunen–Loéve transform (Jackson *et al.* 1991). De Franco & Musacchio (2001) assume that the elliptically polarized signal energy is mainly on the first two principal axes and construct the filtered signals **F** of the triaxial system from a weighted sum of the first two eigenimages $\mathbf{E}_1$ and $\mathbf{E}_2$:

$$\mathbf{F} = (\mathbf{E}_1 \cdot R_1 + \mathbf{E}_2 \cdot R_2) \cdot P \tag{7}$$

where R_1, R_2 and P are the rectilinearities along the first and second principal axes, and the planarity, respectively. The authors obtain these values from the eigenvalues on non-overlapping windows and cubic spline interpolation. Their method enhances linear and elliptical motion through the weights and the omitting of the third eigenimage, which should be dominated by noise.

We modify their approach using overlapping windows for the weights and eigenimages and ascribe a power (ν) to the weights R_1, R_2 and P in eq. (7). With the power, the importance of the weights can be raised to further clean the records of noise.

For the purpose of comparison, we use the test data from Figs 1(a) and (b). The vertical component filter output for different window lengths and power values are shown in Fig. 8. The traces with $\nu = 1$ correspond to the filter published by De Franco & Musacchio (2001) and show what is generally accepted for most principal-component filters: longer windows are required to suppress the large-amplitude noise, and signal 4 is not separated from its large-amplitude random coda. The use of large power values, however, raises the sensitivity and enables more effective noise suppression. In particular, with short windows, large power values are required. The combination of large power values and short windows permits separation of signal 4 from its large-amplitude noise coda. Although the eigenapproach is amplitude biased, the weights of the large-amplitude noise are still slightly smaller than for the signals, which justifies the use of the power. At long windows, signal 4 is not resolved due to its large-amplitude coda, which already dominates at the end of the signal for 21 sample windows.

In Fig. 9, we show the mean energy ratios for 40 different random noise realizations with signal amplitude spectrum. It proves the importance of the introduction of the power value. Short windows should be used with large power values. The trade-off between window size and power can be used to improve the signal resolution. This is helpful when there is small signal separation and/or large noise. We expect that the reported trade-off holds for other polarization filters with weight functions.

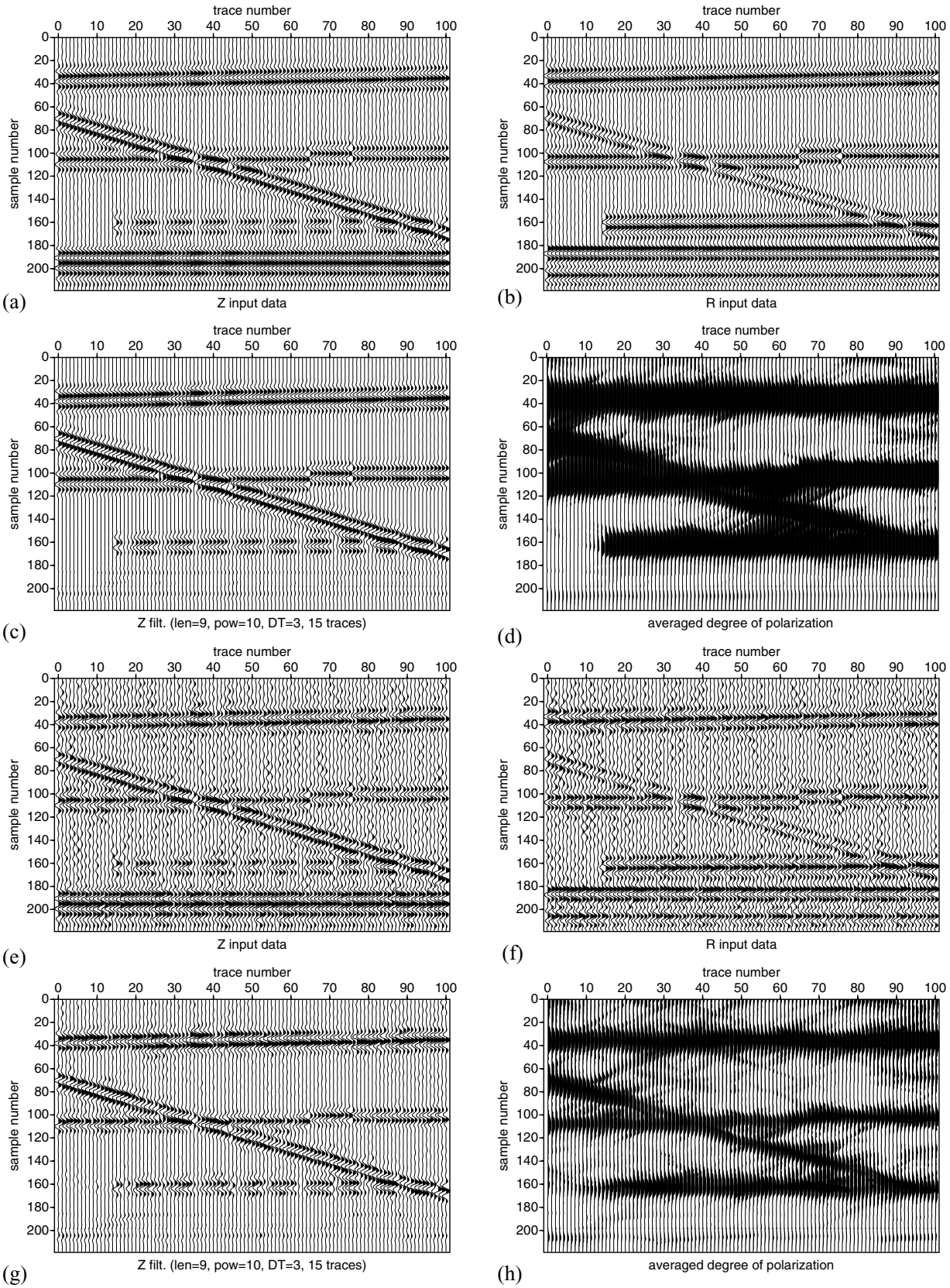

Figure 7. Vertical component (a) and radial component (b) input data to test the spatial averaging procedure. The first arrival has elliptical polarization with changing phase (3°/trace). The other signals have circular, linear or elliptical polarization. Signals and noise have the same frequency spectrum. After sample 179 the data consist of spatially coherent noise. The corresponding vertical component filter result and the averaged degree of polarization are shown in (c) and (d). The spatial averaging does not punish the abrupt and continuous waveform changes. Parts (e)–(h) show the data with greater noise contamination and the corresponding filter results.

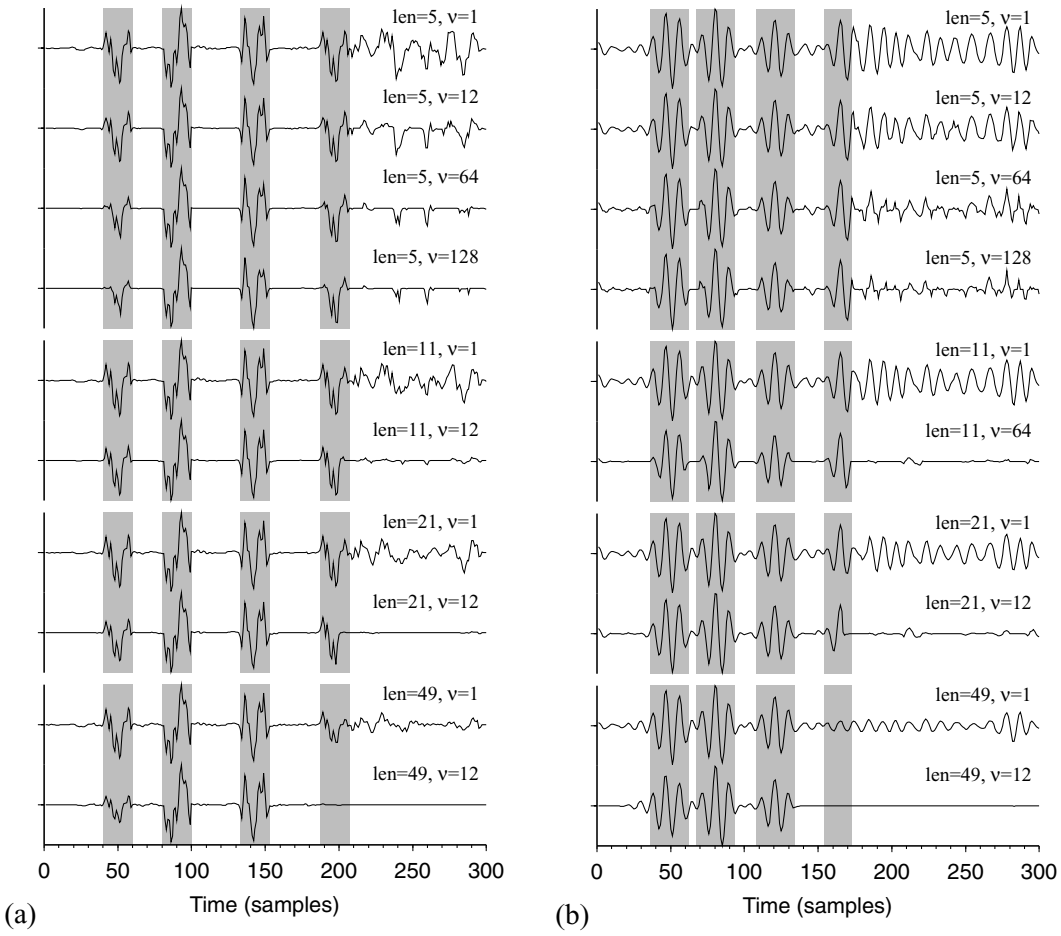

Figure 8. The test data from Figs 1(a) and (b) have been filtered using the weighted eigenimage approach and various filter settings. The vertical component filter output is demonstrated in (a) and (b) for the *bb* and *nb* data, respectively. The traces with $\nu = 1$ correspond to the filter suggested by De Franco & Musacchio (2001). Long windows ($\nu = 1$) are required to suppress the large-amplitude noise which also attenuate signal 4. The introduction of the power relationship helps to reduce the noise. This permits resolution of signal 4 at smaller window lengths.

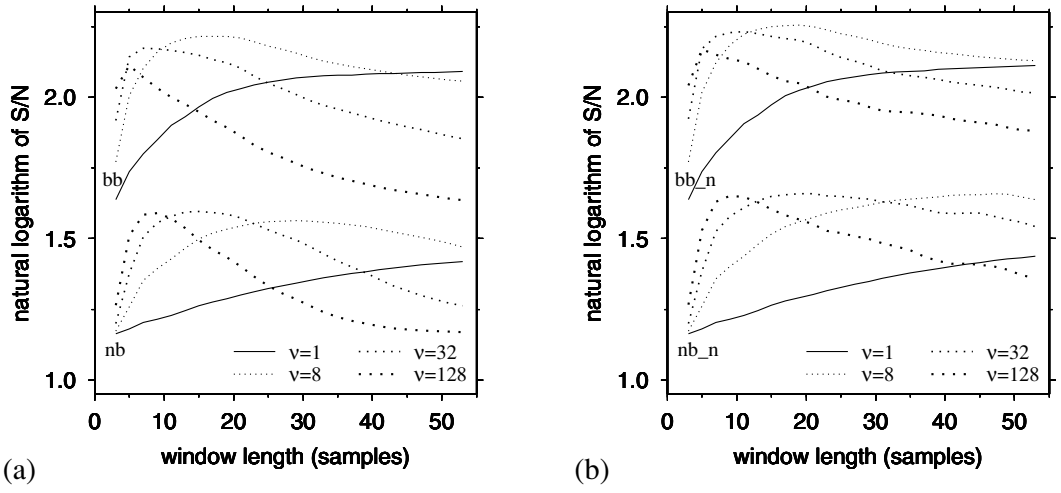

Figure 9. (a) Signal-to-noise energy ratio as a function of data window and power for the weighted eigenimage filter. (b) Same as (a) but the filter output has been normalized. The introduction of the power relationships improved the filter efficiency at shorter window lengths which enables improved signal resolution.

4 REAL DATA EXAMPLES

In the following we test the performance of our filter with data from one Ligurian Sardinian wide-angle seismic profile acquired during 1995 in the Western Mediterranean. The record section used comes from profile 5 in Gallart *et al.* (2001) and was recorded at the coast on station C. The air-gun shots were separated by about 50 m and the corresponding wavefields were recorded with a sample

interval of 16 ms in the easternmost Pyrenees. The objective was the study of the onshore–offshore crustal transect at the eastern Pyrenees (see Gallart *et al.* 2001, for details). Here we focus on the filter performance and do not discuss the structural implications.

4.1 Example without spatial averaging

Figs 10(a)–(c) show the 5–10 Hz bandpassed three-component recordings. No data stacking or other processing are applied to diminish noise. Every 40th trace of the record section is plotted, the traces are balanced with their rms (root-mean-square) amplitude, and a reduction velocity of 6 km s^{-1} is used. The vertical component record section is also shown with a higher record density in Figs 11(a) and (c).

At the smaller distances the data contain a refraction from the basement (P_g) and, as the strongest features reflections from the Moho boundary (*PmP*). Refractions and reflections at other boundaries have been detected. They are, however, smaller in amplitude and are not visible in this data representation. Beyond 70 km offset, noise seems to dominate the recorded section. The data in Fig. 10 show little spatial coherence due to the record decimation to about 2 km trace spacing, as well as heterogeneities and the presence of noise.

Subsequent panels in Fig. 10 contain the vertical component data. All the filtered traces are balanced by the rms values of the unfiltered vertical component data. Spatial averaging procedures or other algorithms are not applied. The seismograms obtained with our degree of polarization filter are shown in Figs 10(d)–(f). Panels 10(g)–(i) illustrate three different outputs using the modified weighted eigenimage approach by De Franco & Musacchio (2001). The power and the window length are indicated below each panel. All filtered sections show noise reduction. Beyond 70 km offset, many isolated signals are visible. These are mostly attenuated noise but are visible due to the trace balance. Isolated polarized signals

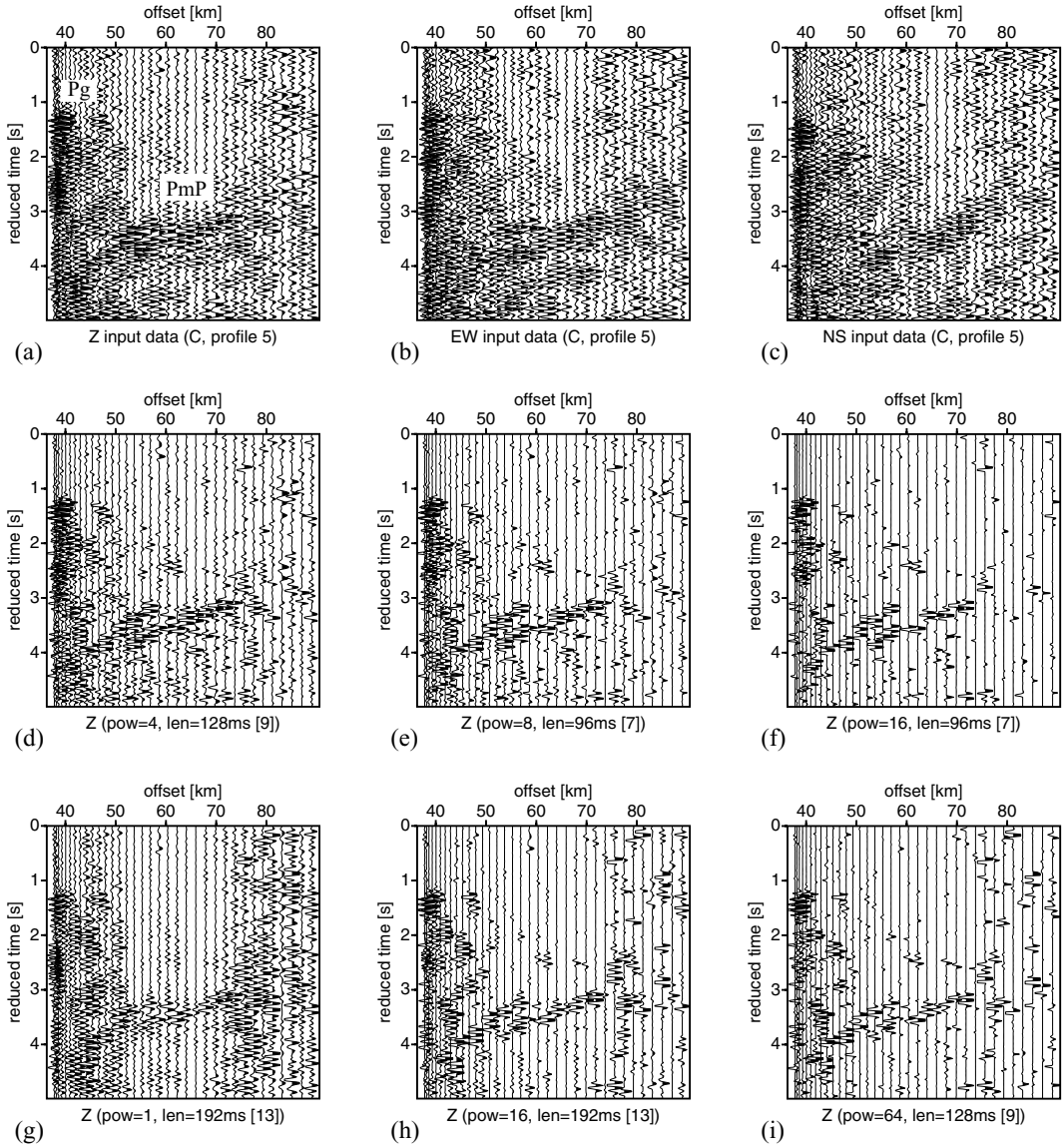

Figure 10. Every 40th record from profile 5, station C is used to increase the seismogram visibility. The 5–10 Hz bandpassed three-component recordings are shown in (a)–(c). The traces in (d)–(f) are from the degree of polarization filter. Parts (g)–(i) show three different outputs of the eigenimage filter. The numbers in square brackets are the number of samples in the moving data windows.

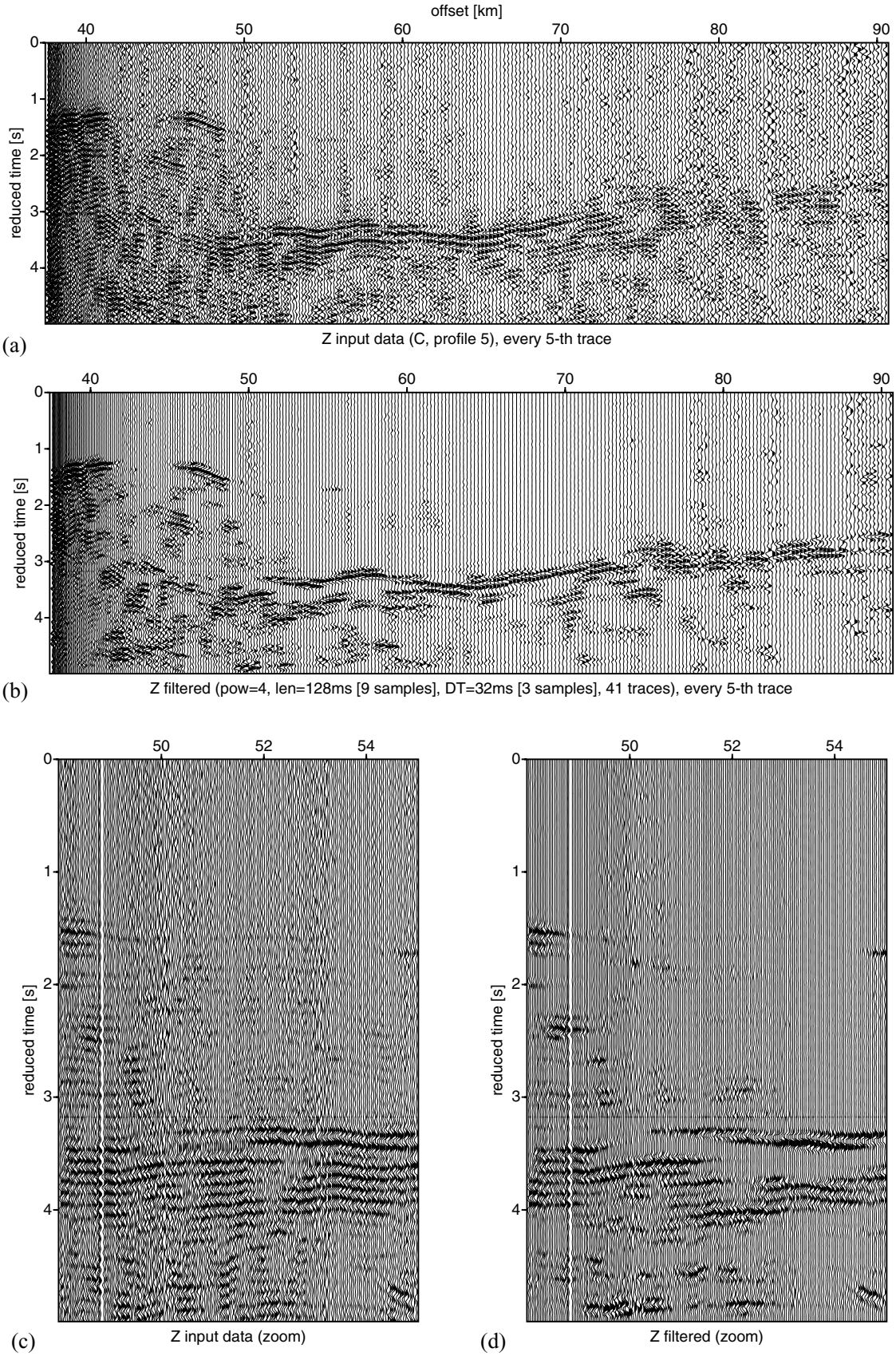

Figure 11. (a) The record section contains every fifth trace of the vertical component bandpassed input data. The complete data set is filtered with the instantaneous degree of polarization filter and every fifth trace is shown in (b). The number of traces for the spatial averaging refers to the complete data set. Parts (c) and (d) show a zoom into the complete vertical component record section.

in a dense record section are probably noise and can be suppressed when employing a spatial averaging of the instantaneous attributes $c(\mathbf{a}(t), \mathbf{p}(t))$. In the following we show that the inclusion of spatial information greatly improves the signal detection by the polarization.

4.2 Example with spatial averaging

We use the complete data set from profile 5, station C to show the filter performance with spatial averaging of the instantaneous degree of polarization. The median is used in all examples. Fig. 11(a) shows every fifth vertical component record of the data set. The only processing is a 5–10 Hz bandpass filter. To improve the visual appearance of the data, the traces are normalized using their rms values. Fig. 11(c) shows a detailed subsection of the complete data set. The filtered data are shown in Figs 11(b) and (d). We use the power $\nu = 4$ and an analysis window of nine samples (128 ms) for the polarization analysis. 41 traces have been used in the local averaging with a three-sample time window ($\Delta T = 32$ ms).

An overall noise reduction is clearly visible in the filtered record section. At distances larger than 70 km the *PmP* phase has been particularly enhanced through attenuation of surrounding noise. At distances smaller than 50 km, the record section is dominated by various reverberations that start at the P_g phase and which cause spatially coherent coda signals (Fig. 11c). A local slant stack would have enhanced all spatially coherent signals while inclusion of the polarization (Fig. 11d) suppressed the less polarized portions of the coda.

The *PmP* phase is not visible as a spatially coherent signal throughout the record section. This has also been observed further south at the Valencia trough (Gallart *et al.* 1994). The absence may be attributed to topography and other complexities as responses to deep crustal faulting during the different tectonic episodes that affected the NE Iberian–Mediterranean transition (Gallart *et al.* 1994, 2001). Note that the filter did not taper these complexities since the averages are determined by the instantaneous degree of polarization functions.

The filter results are controlled by the filter settings, which depend on the data processor, his/her experience, goals and data constraints. Fig. 12, therefore, shows various other results obtained with more conservative (a) to very aggressive settings (d). With the more aggressive settings of Fig. 12(d), only the most polarized signals are visible. Everything else has been attenuated and causes the image to look very rough. Signals that are slightly less polarized are thus also completely suppressed. The conservative settings diminish much less of the information content of the seismogram section and start to gently enhance the polarized features. We recommend starting by using the filter with various conservative settings and proceeding by changing the settings in response to the data and goals. In this way, the information content is reduced until robust signals are found and can be interpreted.

5 DISCUSSION

In this study, signal-to-noise ratio discrimination is based on the stability of an instantaneous polarization state throughout the signal. For this purpose, we define a degree of polarization estimator for triaxial seismic data systems which we use to build an image enhancement tool. The degree of polarization is invariant under seismogram component rotation since it is built from the projections of the semi-major and planarity vectors on to their mean directions. Consequently, the signals can be recorded in any spatial orientation. This is an advantage with respect to single-component signal processing, which often requires rotation to achieve the best S/N ratio. Furthermore, the degree of polarization is independent of the waveform and the type of polarization. Therefore, the spatial averaging of this measure does not punish signals that are polarized with spatially changing waveform characteristics. Conversely, conventional waveform and covariance matrix averaging attenuates polarized signals with spatially changing properties. Spatially coherent but less polarized signals can be attenuated, which makes this method suitable for suppressing signal-generated noise such as less polarized coda reverberations.

Since our filter is a time-domain multiplication of the time-series by an attribute with amplitude between 0 and 1, signals can only be more or less attenuated. Thus, spatial averaging of the instantaneous degree of polarization cannot alter the signal polarity. What may happen is that noise sandwiched between polarized signals is not attenuated during the averaging. This can be solved with shorter windows or other post-polarization analyses. Nevertheless, it may also be a welcome feature: the spatial averaging can act as an image restorer, attenuating isolated polarized signals and avoiding the suppression of features that are less polarized due to unfortunate placement between a suite of polarized signals. This also holds at the crossing of reflections. At a point where signals interfere, the filter without attribute averaging may attenuate the signals conforming their polarization, whereas the averaging can preserve the crossing of reflections.

There are different ways to average. We prefer to use the median, which is a non-linear average with little blurring and is robust with respect to amplitude outliers. Generally, some averaging in polarization analyses is appropriate for improving signal resolution (Bataille & Chiu 1991; Jurkevics 1988, and others). However, averaging can be difficult for complex wavefields due to spatial lag and decreased signal correlation (Christoffersson *et al.* 1988).

Note that our filter is not designed to reconstruct the polarized signal waveforms. No statistical noise estimation is employed and the noise-corrupted signals are simply attenuated based on their polarization. More polarized signals are enhanced relative to less polarized signals and noise as long as the differences in their corresponding degree of polarization values are sufficiently large. Otherwise, the signal is excessively corrupted and therefore attenuated as noise. The time domain is not a good choice for separating these signals from noise. Methods based on various philosophies should be applied to reveal them, for instance, in the frequency domain and with noise estimates from windows prior to the signal arrival time (Du *et al.* 2000).

An alternative definition of the degree of polarization is given by Samson & Olson (1980). They seek polarized signals with one (or two) non-zero eigenvalues of the spectral matrix and construct a corresponding degree of polarization. Their frequency-dependent measure weights the Fourier transform in the sliding data window of a data-adaptive polarization filter (Samson & Olson 1981). The frequency-dependent degree of polarization acts as a bandpass filter, that is, it suppresses the less polarized frequency components.

Different weighting functions have been designed, generally from principal-component attributes (for example, Montalbetti & Kanasewich 1970; Bataille & Chiu 1991; Perelberg & Hornbostel 1994; Morozov & Smithson 1996) and are used as directional and/or pre-defined polarization filters. Their weighting functions can suppress signal-generated noise such as out-of-plane arrivals and ground roll or can separate *P*-to-*S* conversions. Bai & Kennett (2000) use the low gradient of signal strike and the difference

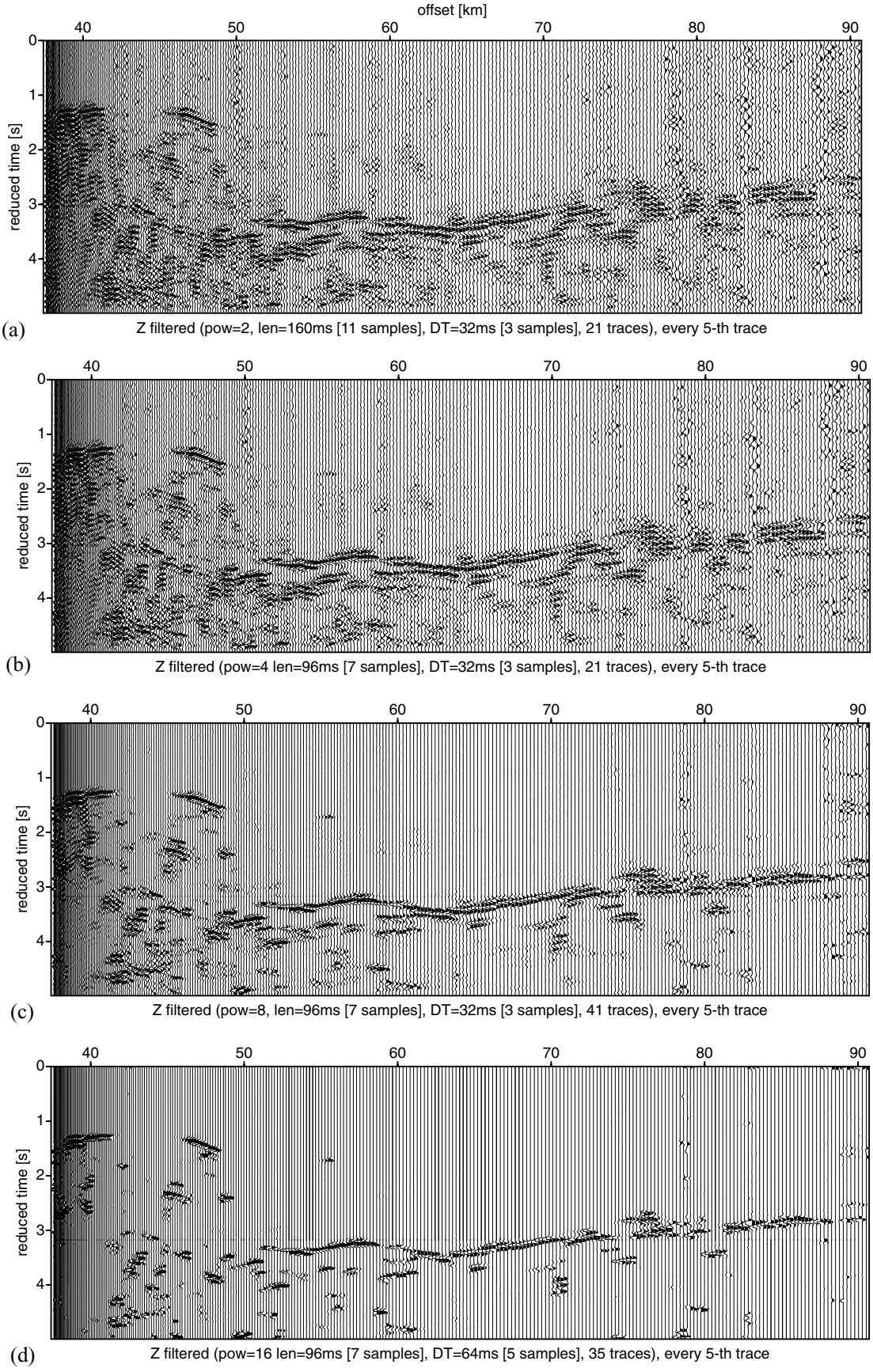

Figure 12. Four distinct degree of polarization filter results are shown. We use the complete data set (station C, profile 5) with moderate (a), (b) to more aggressive (c), (d) filter settings. Sections (a)–(d) contain every fifth record.

between linear and elliptical polarization to aid their body wave signal detector. Many other weighting systems have been constructed, most of which enhance linear motion.

Linear signals can be recorded as elliptical signals due to noise and structural complexities (Perelberg & Hornbostel 1994; Wagner & Owens 1996) and would be attenuated by a filter relying on rectilinearity or other measures of degree of linear polarization. These problems are bypassed in our approach. Another concern is the explicit noise energy bias of the diagonal elements of the covariance matrix (for example, Perelberg & Hornbostel 1994; Schimmel 1999). The degree of polarization method presented here uses amplitude normalized vectors and is therefore explicitly amplitude unbiased. The presence of large energy noise within the analysis window is therefore less disturbing in our approach. However, if no large energy noise is expected and if the preservation of large-amplitude signals is more important, then the use of an amplitude-biased measure can be the better choice. The polarization of large-amplitude signals is less vulnerable to noise than is that of smaller signals. We therefore also present an amplitude-biased degree of polarization functional. The same concept can also be employed with more specialized low-pass filters to determine the mean vector from the optionally normalized semi-major and planarity vectors.

The eigenmethod of De Franco & Musacchio (2001) is a filter which performs the principal-component transform using a SVD method. The combination of planarity and linearity weighting functions permits detection of linear and elliptically polarized motion. We attach a power to their weight functions and show that similarly to our approach, there exists a window length against power trade-off that can be exploited to increase the signal resolution. On the one hand, the data windows must be long enough to discriminate between signals and noise, but on the other hand, only one signal should be included within any window. The power value permits use of shorter windows to prevent inclusion of other signals and additionally increases the efficiency of noise suppression. We consider that this trade-off can be an important option in many principal-component filters, especially with noisy data.

Note that our filter presents an alternative to principal-component filters thanks to the analytic vector definition of Morozov & Smithson (1996). The filter concept is straightforward and easily applied to other formalisms such as the eigenanalysis, which, in general, plays an important role in the analysis of multicomponent multichannel data. The advantages of our time-domain approach are: the time windows are short giving better signal resolution, no noise estimation is required, the method is robust with respect to large-amplitude noise in the vicinity of the signal, a waveform-independent spatial averaging is enabled and permits attenuation of isolated polarized noise but prevents the attenuation of isolated unpolarized signals.

6 CONCLUSIONS

A new objective measure for the degree of polarization is shown to be useful both as a filter and an image enhancement tool. The instantaneous attribute is independent of the orientation of the triaxial seismic data system and handles linear and elliptically polarized signals. The measure can be constructed from short data windows and does not need the eigenanalysis of a data covariance matrix. The degree of polarization is defined to be independent of signal energy, although an amplitude-biased alternative is also given.

For seismic record sections, the degree of polarization is averaged over space to suppress isolated polarized features. The median is used since it is robust to noise bursts with minimal blurring of sharp detail. Filter records are obtained by time-domain multiplication of the instantaneous degree of polarization with the time-series. Since the same function is used for all three components, amplitude ratios are preserved across the triaxial recordings. The waveforms themselves are only preserved when the degree of polarization is constant throughout the course of the signals and this can be forced using a minimum duration algorithm. Since the degree of polarization is explicitly independent of waveform and polarization state, it does not attenuate polarized signals with spatially varying characteristics. This enables, for instance, enhancement of signals reflected near critical angles. Spatially coherent but less polarized signals can be attenuated, which makes this method suitable for suppressing signal-generated noise such as coda reverberations.

Furthermore, combining our approach with a weighted eigenimage filter, it is shown that the optimum window length can be controlled by an exponent of the weighting functions. The trade-off between window and power is important to regulate signal resolution, which depends on window size. We suggest that this concept can be applied to the distinct principal-component filters, which generally require long windows to discriminate between signal and noise energy, to allow them to work more efficiently at shorter windows.

Our approach reduces the information content of the seismograms as a function of the filter settings to find the polarized features. This can significantly improve seismogram interpretation. We suggest starting filtering with conservative settings and proceeding to more aggressive settings as required by the data. The concept of the filter is simple enough to allow for various data-specific optimizations.

ACKNOWLEDGMENTS

The wide-angle data belongs to the LISA margins project and we are grateful to the researchers and technicians who contributed to acquiring these data. We acknowledge the constructive comments of two anonymous reviewers and the thoughtful reading and corrections by the Managing Editor Russ Evans, which improved the manuscript. Plots were made using Generic Mapping Tools (GMT) by Wessel & Smith (1991) and Seismic Unix by Cohen & Stockwell (1999). This research has been supported by the Spanish Ministry of Education, Culture, and Sport through grant SB2000-0120 and by a Marie Curie Fellowship of the European Community programme IHP (HPMF-CT-2001-01322).

REFERENCES

Bai, C.Y. & Kennett, B.L.N., 2000. Automatic phase detection and identification by full use of a single three-component broad-band seismogram, *Bull. seism. Soc. Am.,* **90,** 187–198.

Bataille, K. & Chiu, J.M., 1991. Polarization analysis of high-frequency, three-component seismic data, *Bull. seism. Soc. Am.,* **81,** 622–642.

Christoffersson, A., Husebye, E.S. & Ingate, S.F., 1988. Wavefield decomposition using ML-probabilities in modelling single-site 3-component records, *Geophys. J. R. astr. Soc.,* **93,** 197–213.

Cohen, J.K. & Stockwell, J.W., 1999. *CWP/SU: Seismic Unix Release 33: a Free Package for Seismic Research and Processing,* Center for Wave Phenomena, Colorado School of Mines.

De Franco, R. & Musacchio, G., 2001. Polarization filter with singular value decomposition, *Geophysics,* **66,** 932–938.

Du, Z., Foulger, G.R. & Mao, W., 2000. Noise reduction for broad-band, three-component seismograms using data-adaptive polarization filters, *Geophys. J. Int.,* **141,** 820–828.

Duncan, G. & Beresford, G., 1994. Slowness adaptive f–k filtering of prestack seismic data, *Geophysics,* **59,** 140–147.

Gallart, J., Vidal, N., Dañobeitia, J.J. & the ESCI-Valencia Trough Working Group, 1994. Lateral variations in the deep crustal structure at the Iberian margin of the Valencia trough imaged from seismic reflection methods, *Tectonophysics,* **232,** 59–75.

Gallart, J., Diaz, J., Nercessian, A., Mauffret, A. & dos Reis, T., 2001. The eastern end of the Pyrenees: seismic features at the transition to the NW Mediterranean, *Geophys. Res. Lett.,* **28,** 2277–2280.

Jackson, G.M., Mason, I.M. & Greenhalgh, S.A., 1991. Principal component transforms of triaxial recording by singular value decomposition, *Geophysics,* **56,** 528–533.

Jurkevics, A., 1988. Polarization analysis of three-component array data, *Bull. seism. Soc. Am.,* **78,** 1725–1743.

Kanasewich, E.R., 1981. *Time Sequence Analysis in Geophysics,* University of Alberta Press, Alberta.

Kennett, B.L.N., 2000. Stacking three-component seismograms, *Geophys. J. Int.,* **141,** 263–269.

Kong, S.M., Phinney, R.A. & Roy-Chowdhury, K., 1985. A nonlinear signal detector for enhancement of noisy seismic record sections, *Geophysics,* **50,** 539–550.

Milkereit, D.B., 1987. Decomposition and inversion of seismic data—an instantaneous slowness approach, *Geophys. Prosp.,* **35,** 875–894.

Montalbetti, J.F. & Kanasewich, E.R., 1970. Enhancement of teleseismic body phases with a polarization filter, *Geophys. J. R. astr. Soc.,* **21,** 119–129.

Morozov, I.B. & Smithson, S.B., 1996. Instantaneous polarization attributes and directional filtering, *Geophysics,* **61,** 872–881.

Park, J., Vernon, F.L. & Lindberg, C.R., 1987. Frequency dependent polarization analysis of high-frequency seismograms, *J. geophys. Res.,* **92,** 12 664–12 674.

Perelberg, A.I. & Hornbostel, S.C., 1994. Application of seismic polarization analysis, *Geophysics,* **59,** 119–130.

Reading, A.M., Mao, W. & Gubbins, D., 2001. Polarization filtering for automatic picking of seismic data and improved converted phase detection, *Geophys. J. Int.,* **147,** 227–234.

Samson, J.C., 1983. The spectral matrix, eigenvalues, and principal components in the analysis of multichannel geophysical data, *Ann. Geophys.,* **1,** 115–119.

Samson, J.C. & Olson, J.V., 1980. Some comments on the descriptions of the polarization states of waves, *Geophys. J. R. astr. Soc.,* **61,** 115–130.

Samson, J.C. & Olson, J.V., 1981. Data-adaptive polarization filters for multichannel geophysical data, *Geophysics,* **46,** 1423–1431.

Schimmel, M., 1999. Phase cross-correlations: design, comparisons and applications, *Bull. seism. Soc. Am.,* **89,** 1366–1378.

Schimmel, M. & Paulssen, H., 1997. Noise reduction and detection of weak, coherent signals through phase weighted stacks, *Geophys. J. Int.,* **130,** 497–505.

Stoffa, P.L., Buhl, P., Diebold, J.B. & Wenzel, F., 1981. Direct mapping of seismic data to the domain of intercept time and ray parameter—a plane-wave decomposition, *Geophysics,* **46,** 255–267.

Taner, M.T., Koehler, F. & Sheriff, R.E., 1979. Complex seismic trace analysis, *Geophysics,* **44,** 1041–1063.

Vidale, J.E., 1986. Complex polarization analysis of particle motion, *Bull. seism. Soc. Am.,* **76,** 1393–1405.

Wagner, G.S. & Owens, T.J., 1996. Signal detection using multi-channel seismic data, *Bull. seism. Soc. Am.,* **86,** 221–231.

Wessel, P. & Smith, W.H.F., 1991. Free software helps map and display data, *EOS, Trans. Am. geophys. Un.,* **72,** 441, 445–446.